J. Synchrotron Rad. (1998). **5**, 908–910

DAFS measurements using the image-plate Weissenberg method

Naoya Sugioka,[a]* Kenji Matsumoto,[a] Masahiko Tanaka,[b] Takeharu Mori[b] and Satoshi Sasaki[a]

[a]Materials and Structures Laboratory, Tokyo Institute of Technology, Nagatsuta 4259, Midori, Yokohama 226-8503, Japan, and [b]Photon Factory, National Laboratory for High Energy Physics, Oho 1-1, Tsukuba 305-0801, Japan. E-mail: sasaki@n.cc.titech.ac.jp

(*Received 4 August 1997; accepted 9 January 1998*)

An instrumental technique for DAFS measurements which can provide site-specific information is proposed. The approach uses (i) focusing optics with parabolic mirrors and a double-crystal monochromator, (ii) the Laue and Bragg settings and (iii) data collection by the image-plate Weissenberg method. Six image exposures are recorded per plate at five intrinsic energies and one reference energy. The single-crystal measurements were performed at the Co *K*-absorption edge, and the 200, 220 and 311 reflections of CoO and 511 and 911 reflections of Co_3O_4 were used for analysis. The regression analysis of $\chi(k)$, Fourier transforms of $k^3\chi(k)$ and back-Fourier filtering have been performed.

Keywords: diffraction anomalous fine structure (DAFS); CoO; Co_3O_4.

1. Introduction

X-ray diffraction and X-ray absorption spectroscopies are currently used for structural analyses. The former gives long-range information on the crystal structure, whereas the latter gives localized structural information on a specific element. DAFS (diffraction anomalous fine structure) gives the intensity of an X-ray diffraction spot as a function of the incident X-ray energy which is scanned through an absorption edge. DAFS may give a linear combination of XAFS (X-ray absorption fine structure) modulations and of their Kramers–Krönig transforms. It provides long-range structural information and short-range spectroscopic information with useful information on both site and valence selectivity. Recently, the DAFS technique has been developed as a combined spectroscopic and crystallographic method using synchrotron radiation (Arcon *et al.*, 1987; Stragier *et al.*, 1992; Bazin & Sayers, 1993*a*,*b*; Bouldin *et al.*, 1993; Pickering *et al.*, 1993*a*,*b*; Tweet *et al.*, 1993; Lee *et al.*, 1994; Vacinova *et al.*, 1995, 1996; Hodeau *et al.*, 1995). The DAFS approach is similar in concept to the polychromate profile method of Arndt *et al.* (1982) tested on the rhenium L_{III}-edge. The fundamentals of the procedure using the DAFS method have been reviewed (Mizuki, 1993; Sorensen *et al.*, 1994).

We present here a methodology using the Weissenberg method which allows DAFS data to be collected for many reflections simultaneously, in the Laue case as well as the Bragg case even under severe absorption. It is also possible to observe Bragg spots on an image plate with a series of scans of 50–100 energy steps. Such an experimental set-up allows shorter data-collection time and higher performance since a two-dimensional detector is used. There is no extra diffractometry setting required with an X-ray energy scan.

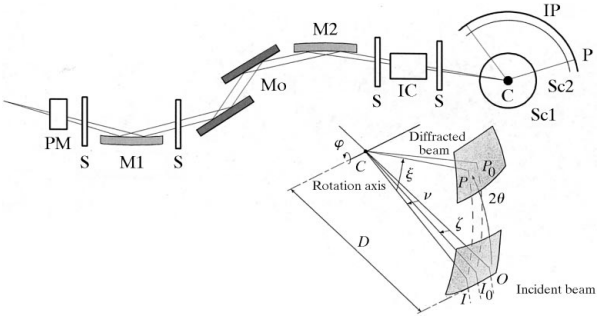

Figure 1
Experimental set-up and diffraction geometry of the Weissenberg camera: PM, beam-position monitor; S, slit; M1, M2, mirrors; Mo, monochromator; IC, ionization chamber; C, crystal; Sc1, Sc2, screens; IP, image plate. The reciprocal lattice coordinates (x, y, z) can be described in the camera coordinate system (X, Y), where X is parallel to the direction of camera translation and Y is in the radial direction of the cylinder: $x = \cos\nu\cos\zeta - \cos\zeta$, $y = \cos\nu\sin\xi$, $z = \sin\nu - \sin\zeta$, $X = D(\tan\nu - \tan\zeta) + (\varphi - \varphi_1)/K$, $Y = D\xi$. D = camera radius, K = coupling ratio of crystal rotation to camera translation, φ = crystal rotation angle from φ_1 to φ_2.

2. Experimental

Single crystals of CoO and Co_3O_4 were used for the DAFS experiments. The CoO sample (NaCl structure, cubic, $Fm\bar{3}m$, a = 4.263 Å), prepared by the Bernoulli method, was cut into a 0.1 × 0.1 × 0.01 mm plate. The single crystals of Co_3O_4 (spinel structure, cubic, $Fd\bar{3}m$, a = 8.084 Å), ranging from 0.05 to 0.09 mm in one dimension, were grown at 1123 K for 29 h.

All experiments were performed on beamline BL3A at the Photon Factory (Sasaki *et al.*, 1992). A schematic diagram of the experimental set-up is shown in Fig. 1. Optical components including a collimating paraboloidal mirror, a double-crystal monochromator and a focusing paraboloidal mirror made the diffraction experiments with focused X-rays possible. The optics guarantee a smooth variation of photon flux in the X-ray region used. The critical energy of the first Pt-coated fused-quartz mirror was fixed at 20 keV to cut out higher harmonics. In order to reduce the air scattering and absorption, a helium path was installed in the experimental hutch.

Diffraction intensity and XAFS absorption data are collected at each energy step in the vicinity of the Co *K*-edge. The X-ray energy was calibrated by measuring the absorption edge of cobalt foil. The DAFS intensities for the Bragg diffraction spots were recorded on the image plate of a Weissenberg camera. The energy range and step intervals are based on a standard XAFS measurement at the electron binding energy E_0 (7709.3 eV) and the energy resolution of the photons. A reference energy (E_{std} = 7694.1 eV) was used for intensity normalization. An ionization chamber was used for correcting variations in incident X-ray beam intensity.

The use of an area detector is preferred since the scattering angle changes with X-ray energy. Because current electronic area detectors are limited either in counting characteristics or detector size, the image plate, a BaFBr:Eu^{2+} photostimulable phosphor screen, was chosen for its high sensitivity and its dynamic range of 1:10^5 (Sonoda *et al.*, 1983; Miyahara *et al.*, 1986). A new type of Weissenberg camera was designed for these experiments, which is

a screenless as well as a conventional screen-on Weissenberg camera. A different type of screen (Sc2 in Fig. 1) can also be employed to lower the background level. The oscillation and Weissenberg photographs were taken using a film translation parallel to the spindle axis. Multiple exposure measurements were used with the film translation perpendicular to the spindle axis. The Weissenberg geometry and detector coordinates are described in Fig. 1 (Higashi, 1989). The distance from the crystal sample to image plate (camera radius) was 171.9 mm. The image plates were produced by Fuji Film Co. Ltd, with a size of 400 × 200 mm and 0.1 × 0.1 mm pixels.

We have developed a method to process the diffraction data taken by the image-plate Weissenberg camera. Six different energy images, including an image at $E_{\rm std}$, were recorded at 1° intervals along the radial direction of the cassette cylinder. The data collections for the CoO and Co_3O_4 samples were carried out within a spindle-angle rotation of 50° and 30°, respectively. The measuring times for each exposure were 2.5 min and 1.5 min, respectively.

In order to increase the signal-to-noise ratio in the region of severe absorption, the following techniques were introduced: (i) insertion of a noise-reducing screen (Sc2) between the sample and the image plate, (ii) insertion of a normal cassette screen (Sc1) in the case where only either zero- or upper-layer photographs are taken, and (iii) reduction of the exposure repetition. The X-ray energy regions for the measurement of Co *K* DAFS spectra overlap with those of the Eu $L_{\rm I}$-, $L_{\rm II}$- and $L_{\rm III}$-edges. It was clear in our experiments that there was a small energy dependence of the response of the image plate in the energy region E = 7–9 keV.

Data analysis was made using a BAS2000 image-plate readout system at the Photon Factory. Single crystals with well known structure were chosen in this study to isolate the fine-structure oscillations as test systems. Indexing of the observed Bragg reflections was successfully made in accordance with the Weissenberg geometry. The 200, 220 and 311 reflections of CoO and 511 and 911 reflections of Co_3O_4 were selected for analysis. The following corrections were made: (i) background correction; (ii) normalization of the intensity variation of the incident synchrotron radiation beam; (iii) standardization in intensity using the 311 standard reflection; (iv) fading correction for the exponential polynominals; (v) corrections for the Lorentz factor and absorption effect; (vi) removal of any Bragg glitches; (vii) correction for the variation in the counting efficiency between image plates. The polarization factor was assumed to be unity because the observed spots deviated with small angles from a vertical diffraction plane. The background-subtracted and normalized DAFS spectra for the 200 and 220 reflections of CoO are shown in Fig. 2. The diffracted intensities were well described by the kinematical approximation.

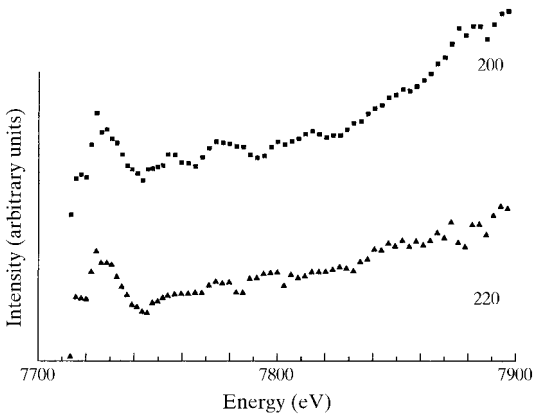

Figure 2
DAFS signals for the 220 and 200 reflections of CoO.

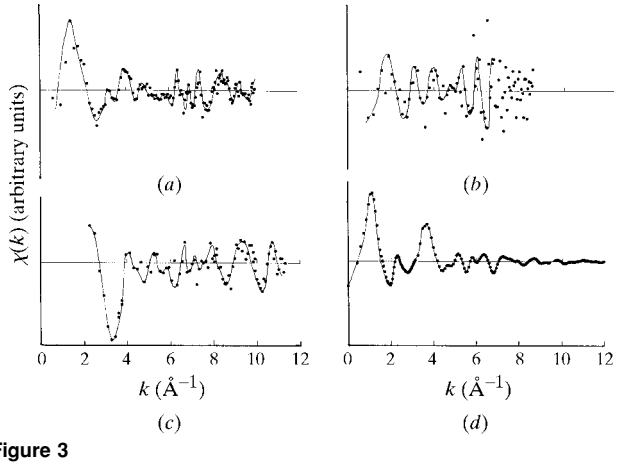

Figure 3
The normalized $\chi(k)$ oscillation functions *versus* k: (*a*) 200 DAFS of CoO, (*b*) 311 DAFS of CoO, (*c*) 911 DAFS of Co_3O_4 and (*d*) XAFS of CoO.

3. Results and discussion

Regression analysis was applied to the measured DAFS intensity instead of the spline method. The regression function is given by

$$y = \sum \beta_j x^j + \varepsilon \quad (j = 0, 1, ..., n),$$

where β is the regression coefficient, ε is an error term and x is a variable. The DAFS spectra were then split into two functions at the node of the oscillation function. Each of the functions was fitted in the analysis of covariance. The χ functions obtained for CoO are shown in Fig. 3.

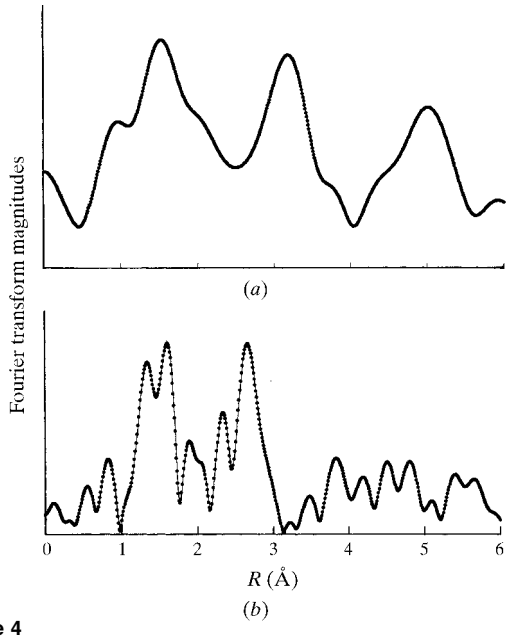

Figure 4
The Fourier transform magnitudes of (*a*) the 200 DAFS and (*b*) XAFS signals *versus* the transform radial distance *R*. The DAFS and XAFS Fourier transform magnitudes are nearly identical except for the phase shift effects.

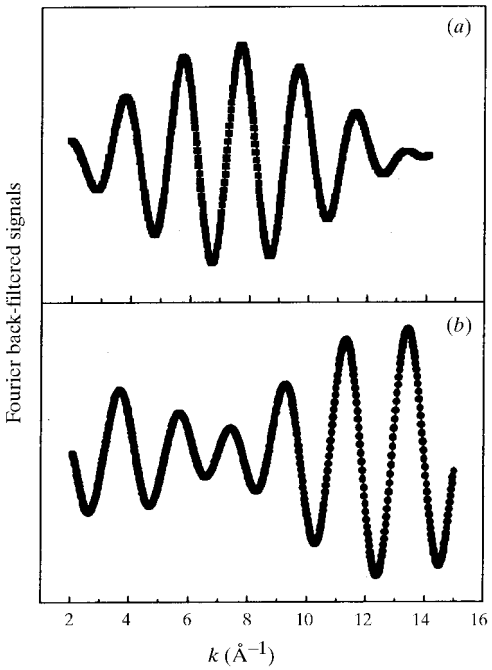

Figure 5
The Fourier back-filtered first shells of (*a*) 200 DAFS and (*b*) XAFS signals, where the peak region is defined as 1.2–1.8 Å (DAFS) and 1.2–1.75 Å (XAFS).

Fourier transforms of $k^3\chi(k)$ were carried out over the wavenumber range $0.6 \leq k \leq 16.8$ Å^{-1}, by using the *EXAFSH* computer program (Yokoyama *et al.*, 1994). Fig. 4 shows the radial structure function of CoO obtained from the 200 reflection DAFS, compared with that from XAFS. The phase shifts between DAFS and XAFS can be determined from the back-filtered data sets when atomic bond distances are invariable. In order to analyse the correlation between the DAFS and XAFS spectra, the Fourier back-filtering method was applied for the first and second shells of the signals shown in Fig. 4 without any constraint on atomic distances. The results are shown in Fig. 5, which has a clear phase shift for the 200 Bragg reflection.

We thank Mr Kazuki Ito at the Photon Factory for his help with the image plate. This study was performed under the auspices of the Photon Factory (PAC No. 96G086). This work was supported in part by a Grant-in-Aid (07805001) and JSPSRFTF96P00205.

References

Arcon, I., Kodre, A., Glavic, D. & Hribar, M. (1987). *J. Phys. C*, **9**, 1105–1108.
Arndt, U. W., Greenhough, T. J., Helliwell, J. R., Howard, J. A. K., Rule, S. R. & Thompson, A. W. (1982). *Nature (London)*, **298**, 835–838.
Bazin, D. C. & Sayers, D. A. (1993*a*). *Jpn. J. Appl. Phys. Suppl.* **32**(2), 249–251.
Bazin, D. C. & Sayers, D. A. (1993*b*). *Jpn. J. Appl. Phys. Suppl.* **32**(2), 252–254.
Bouldin, C. E., Woicik, J. C., Stragier, H., Cross, J. O., Rehr, J. J. & Sorensen, L. B. (1993). *Jpn. J. Appl. Phys. Suppl.* **32**(2), 198–202.
Higashi, T. (1989). *J. Appl. Cryst.* **22**, 9–18.
Hodeau, J. L., Vacinova, J., Garreau, Y., Fontaine, A., Hagelstein, M., El Kaim, E., Lauriat, J. P., Prat, A. & Wolfers, P. (1995). *Rev. Sci. Instrum.* **66**, 1499–1501.
Lee, P. L., Beno, M. A., Knapp, G. S. & Jennings, G. (1994). *Rev. Sci. Instrum.* **65**, 2206–2209.
Miyahara, J., Takahashi, K., Amemiya, Y., Kamiya, N. & Satow, Y. (1986). *Nucl. Instrum. Methods A*, **246**, 572–578.
Mizuki, J. (1993). *J. Jpn. Soc. Synchrotron Rad. Res.* **6**, 309–322.
Pickering, I. J., Sansone, M., Marsch, J. & George, G. N. (1993*a*). *Jpn. J. Appl. Phys. Suppl.* **32**(2), 206–208.
Pickering, I. J., Sansone, M., Marsch, J. & George, G. N. (1993*b*). *Mater. Res. Soc. Symp. Proc.* **307**, 15–20.
Sasaki, S., Mori, T., Mikuni, A., Iwasaki, H., Kawasaki, K., Takagi, Y. & Nose, K. (1992). *Rev. Sci. Instrum.* **63**, 1047–1050.
Sonoda, M., Takano, M., Miyahara, J. & Kato, H. (1983). *Radiology*, **148**, 833–838.
Sorensen, L. B., Cross, J. O., Newville, M., Ravel, B., Rehr, J. J., Stragier, H., Bouldin, C. E. & Woicik, J. C. (1994). *Resonant Anomalous X-ray Scattering, Theory and Applications.* pp. 389–420. Amsterdam: Elsevier Science.
Stragier, H., Cross, J. O., Rehr, J. J., Sorensen, L. B., Bouldin, C. E. & Woicik, J. C. (1992). *Phys. Rev. Lett.* **69**, 3064–3067.
Tweet, D. J., Akimoto, K., Hirosawa, I., Tatsumi, T., Kimura, H., Mizuki, J., Sorensen, L., Bouldin, C. E. & Matsushita, T. (1993). *Jpn. J. Appl. Phys. Suppl.* **32**(2), 203–205.
Vacinova, J., Hodeau, J. L., Bordet, P., Anne, M., Cox, D., Fitch, A., Pattison, P., Schweggle, W., Graafsma, H. & Kvick, A. (1996). *Mater. Sci. Forum*, **228/231**, 95–100.
Vacinova, J., Hodeau, J. L., Wolfers, P., Lauriat, J. P. & El Kaim, E. (1995). *J. Synchrotron Rad.* **2**, 236–244.
Yokoyama, T., Hamamatsu, H. & Ohta, T. (1994). *EXAFSH*, Version 2.1. University of Tokyo, Japan.